XL CILAMCE
IBERO-LATIN AMERICAN CONGRESS ON COMPUTATIONAL METHODS IN ENGINEERING
NOVEMBER 11-14, 2019
Praiamar Natal Hotel & Convention Natal, RN-BRAZIL

ANALYSIS OF LOCAL TENSILE RUPTURE INFLUENCING SHEAR STRENGTH ON UNIAXIAL TEST MODELLING

Ana Itamara Paz de Araújo
Nayara Belfort Accioli Magalhães
anaitapaz@hotmail.com
ntbelfort@gmail.com
Department of Civil Engineering, Federal University of Pernambuco
Recife, Pernambuco 50670-901, Recife-PE-Brazil
Igor Fernandes Gomes
Leonardo José do Nascimento Guimarães
gomes@ufpe.br
leonardo@ufpe.br
Department of Civil Engineering, Federal University of Pernambuco
Recife, Pernambuco 50670-901, Recife-PE-Brazil

Abstract. Constitutive models are mathematical formulations capable of describing the macroscopic behaviour of an ideal medium. These models result from the application of simplifying hypotheses about the behaviour of the real environment. Therefore, the selection of the constitutive model to be used must be related to the problem to be solved, since it would not be trivial to obtain a single formulation that would allow reaching the general solution for the material behaviour. In this sense, modelling is a feature that describes the behaviour of materials subjected to real stress states, such as uniaxial tests performed in the laboratory. Modelling of this type of test is generally performed through models that describe the shear behaviour of the sample, such as Mohr Coulomb and Drucker-Prager models. However, when observing some experiments in the laboratory, it was verified that there are local tensile zones in the samples, which allows a reduction of the material resistance. In this sense, this article presents a study of a rock sample that was submitted to the Uniaxial laboratory test and its resistance was reduced by the tensile zones. Furthermore, in this work the numerical modelling of this test will be presented and the impact of considering these zones of damage in the sample, the constitutive model adopted in these simulations was the tensile damage.

Keywords: Numerical simulation; Tensile stress zones; Uniaxial test.

1 Introduction

Throughout Soil and Rock Mechanics evolution, several studies have been developed to study the geomechanical behaviour of soils and rocks. Thus, several authors have been investigating the behaviour of these materials through numerical tests and modelling of compressive scenarios (BŁAŻEJCZAK; ŚNIEG; SŁOWIK, 2018; FAKHIMI; HEMAMI, 2017; MATHEUS MONTES PIMENTA; ANDRE CEZAR ZINGANO; FERNANDO ALVES CANTINI CARDOZO, 2016).

Therefore the uniaxial compression test is an essential assay for investigating several rock parameters, such as compressive stress strength, Poisson module and indirect tensile stress strength *(KAKLIS et al.*, 2017).

Therefore, materials resistance parameters has been investigated, besides the influence of geometry (RODRIGUES MARQUES *et al.*, 2017), of cyclic loading (MATHEUS MONTES PIMENTA; ANDRE CEZAR ZINGANO; FERNANDO ALVES CANTINI CARDOZO, 2016) and different materials (KAKLIS *et al.*, 2017). However, it is necessary to pay attention to the presence of tensile stresses in the sample, which can reduce its compressive strength by causing detachment in some regions and reducing the section of the sample. This fact can be observed in (FAKHIMI; HEMAMI, 2017), who treated this phenomenon as lateral dilatance and radial stresses.

According to Fakhimi & Hemami (2017), different causes can be attributed to the material´s dilatance behaviour, such as the existence of defects, pores and micro-cracks, attributing a non-uniform behaviour, generating axial splitting in the sample. Not only Fakhimi & Hemami (2017), but also Holzhausen & Johnson (1979) had investigated this behaviour in samples submitted to uniaxial compression test, these authors cited the occurrence of axial splitting due to induction of lateral tensile stress.

This tensile behaviour in the uniaxial test is not well discussed so far, as the main interest of the test is the investigation of the shear behaviour under compression stresses. Thus, this work presents a numerical modelling of the uniaxial rock test in order to discuss the emergence of tensile stresses during the application of uniaxial compression.

2 Constitutive Model of Traction Damage

Based on the mechanics of continuous damage, proposed by Simó & Ju (1987), the damage is a degradation of the rigidity of the material. Therefore it is understood that the model is based on the irreversible thermodynamic processes and is proposed in a way that describes the previous mechanism of the formation of macro fractures.

Concerning the Traction Damage, Oliver *et al.* (2008) introduced it to the damage model, treating the material differently when subjected to a state of traction or compression. The formulation described in this work can be found more broadly in Sánchez *et al*. (2014).

When the damage is in the regime of tensile stress to the constitutive equations will be described introduced the concept of effective tension of damage in order to describe the behavior of the damaged environment.

As described by Sánchez *et al.*, (2014), the constitutive law of this model is described as follows:

$$\sigma = (1 - d)\bar{\sigma} \tag{1}$$

Since σ is the effective stress, d is the damage variable ($0 \leq d \leq 1$) and $\bar{\sigma}$ is the effective stress of damage, which is given by:

$$\bar{\sigma} = \boldsymbol{C} : \varepsilon \tag{2}$$

Where $\boldsymbol{C}$ is the tensile constitutive elastic. Thus, the constitutive law for this model can be expressed by:

$$\sigma = (1 - d)\bar{\sigma}, \ if \ \overline{\sigma_n} > 0 \quad \text{Tensile state.}$$

$$\sigma = \bar{\sigma}, \quad if \ \overline{\sigma_n} \leq 0 \quad \text{Compression state.} \tag{3}$$

Therefore this model is capable of capturing tensile-induced degradation zones.

3 Finite Interface Elements and Strong Built-in Continuities

The fragmentation technique consists of inserting high aspect ratio elements into the regular finite elements, in order to simulate fracture opening when the medium tensions are in the tensile regime. The peculiarity of the interface element used is a high aspect ratio linear triangle whose kinematics is compared to the kinematics of the approximation of strong discontinuities in mechanical problem modelling, and several works have used this technique (MANZOLI, *et al*., 2012; SÁNCHEZ *et al.*, 2014; MAEDO, 2015; SEIXAS, 2015; CLETO, 2016; MACIEL, 2017 and ARAÚJO, (2019).

The incorporated elements are used to simulate discontinuities in the region. This technique inserts discontinuities into the continuous finite element with deformations located in narrow bands, called weak discontinuities, and the displacements are concentrated as the degradation of the material, in zones of fracture processing, until the complete rupture of the discontinuity, then it develops a discontinuity in the field of displacement, and it is called strong discontinuity (BESERRA, 2015).

4 Numerical Simulations Test Uniaxial

For this article, simulations of the uniaxial compression test were performed using the constitutive model of tensile damage, with the intention of verifying zones of damage caused by traction or dilatation effect, as discussed in (FAKHIMI; HEMAMI, 2017). For this, a finite element mesh was generated using the high aspect ratio and strong discontinuity element techniques.

Then the results are divided into four steps, in the first and second analysis, was inserted in the high aspect ratio finite element mesh a left and right discontinuity successively (section 4.1 and 4.2, respectively), the third analysis the discontinuity was inserted into the lower and upper region of the sample (section 4.3) and finalizing the analyses, a conjugated pair of discontinuities were inserted (section 4.4). Remembering that all discontinuities were inserted using the built-in strong discontinuities technique.

The geometry used for the analysis was the same, changing only the positioning of the embedded elements. This geometry was represented by a vertical section of diameter (D) of 0.04 m and height (*H*) 0.07 m, Figure 1. Following are the parameters of the material modulus of Elasticity (*E*), Poisson (*v*), Tensile Strength (δ_y) and Fracture Energy (G_f), see Table 1.

Finite element mesh with triangular elements with 1 Gauss point on each element and a total of 1059 nodes and 1228 elements.

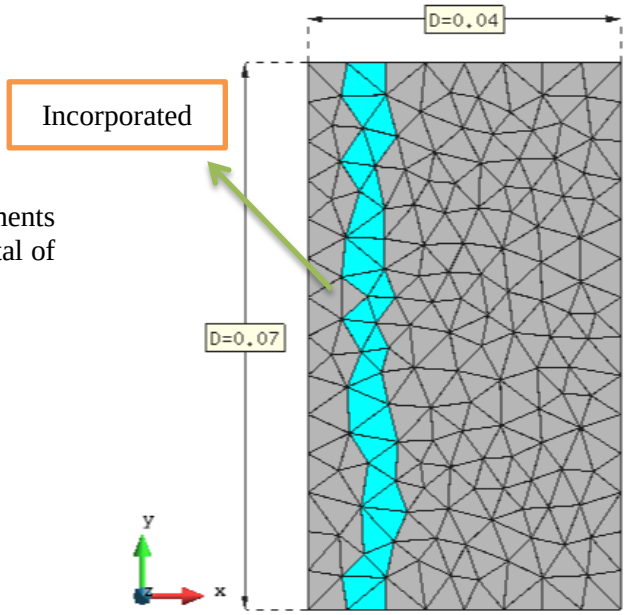

Figure 1. Finite Element Mesh, Uniaxial left Incorporated Element test.

Materials	Modulus of Elasticity $(E)MPa$	Poisson (v)	Fracture Energy $(G_f)N/m$	Tensile Strength $(\delta_y)MPa$
Rock	11675.00	0.35	-----	Elástico.
High aspect ratio element	77.00	0.45	500.00	0.0005
Incorporated	77.00	0.45	500.00	0.05

Table 1. Properties of Materials used in the uniaxial test model, incorporated on the left side.

The boundary conditions were the same for all analyses and can be observed in Figure 2.

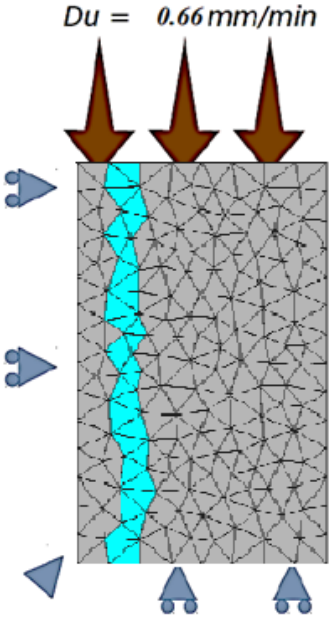

Figure 2. Boundary conditions.

4.1 Uniaxial Scenario 1

In this first scenario the analyses with the vertical discontinuity (Figure 2) on the left side of the sample will be detailed, aiming to verify if in these regions there will be traction zones.

Figure 3 illustrates the field of horizontal 3(a) and vertical 3(b) offsets. In this same figure, it is clear that the displacement field changes with respect to the analysis of Section 4.4, because the discontinuities represent a plane of weakness and these, in this scenario, are positioned vertically.

Thus, it is noted that the sample shows a tendency to negative and positive displacement, in Figure 3(a), representing a tendency to deform the elements in the region near the discontinuity.

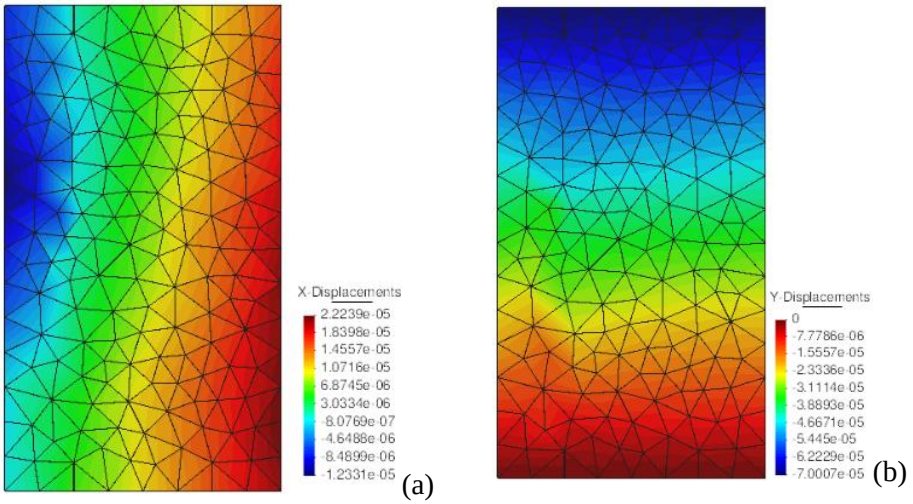

Figure 3. Field of displacement (a) Horizontal and (b) Vertical.

Figure 4 shows the horizontal 4(a), vertical 4(b) and shearers 4(c) stress fields. In this figure it can be observed that the horizontal and vertical tensions are evenly distributed in the elements of the continuum, however, due to the presence of the vertical plane of weakness, Figure 4(b) can be observed the concentration of tensions in the incorporated elements highlighted in red.

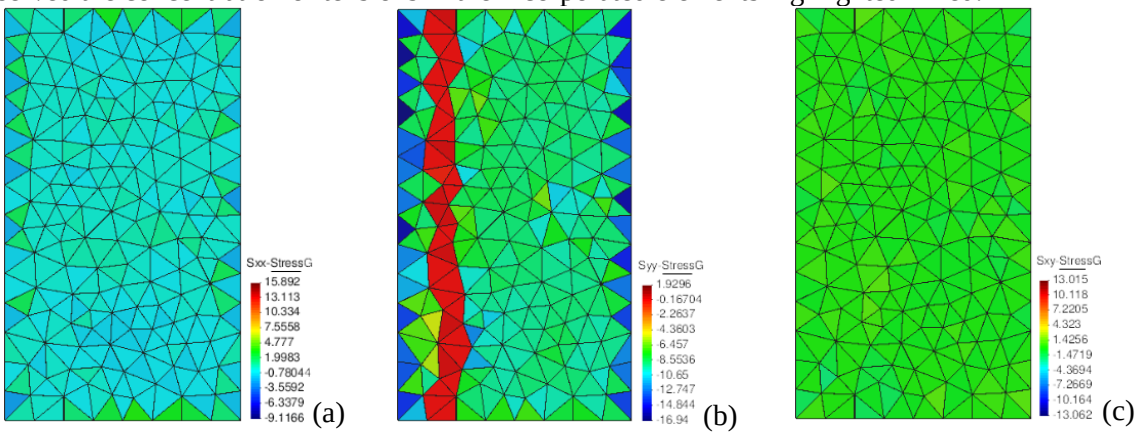

Figure 4. Stress range (a) Horizontal, (b) Vertical and (c) Shearers.

Figure 5 illustrates the effect of damage on the simulation and shows that there were tensile zones in which the material reaches a total rupture (*damage = 1*). Figure 6(a) shows the evolution of the damage during the simulation, with points taken near the degradation region, it is noticed that it evolves during the simulation until it reaches the complete degradation of the material. Figure 6(b) shows the evolution of the fracture opening variable (*hjump n*).

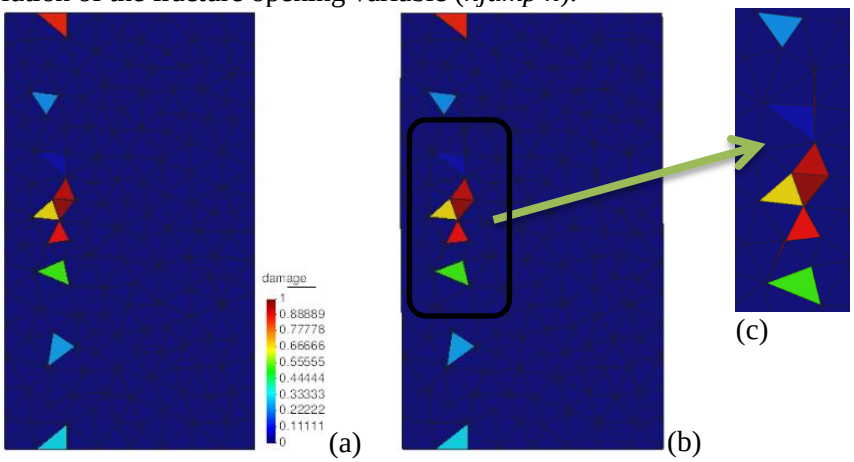

Figure 5. Damage (a) damaged elements, (b) deformed mesh at 30x scale and (c) opening detail.

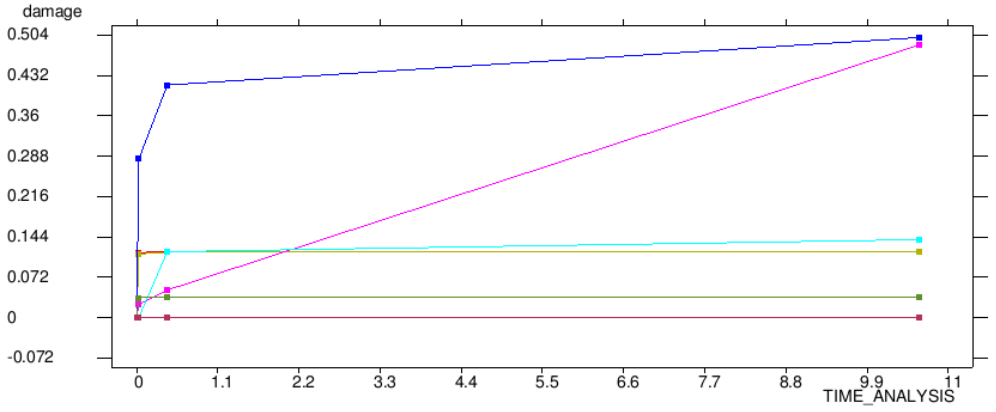

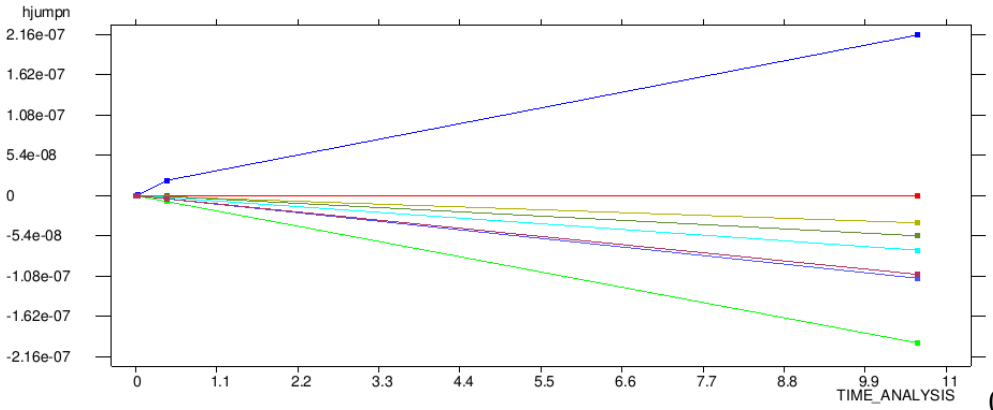

(b)

Figure 6. Evolution of (a) Damage and (b) evolution of aperture variable (*hjump n*) over time.

Figure 7 shows the incorporated discontinuity that is reactivated in elements that reach the value 2 for the "crack elem" variable, that is, material degradation occurs, which mean that there was the dilatance effect. It is noteworthy that in the region where the elements were reactivated is exactly where the effect of fracture dilatation and fracture opening arises, possibly where fractures would arise in the simple compression test in the laboratory. The Figure 7(b) highlights the elements that were analysed in Figure 6(a) and 6(b), it is highlighted that these same elements were analysed in all scenarios.

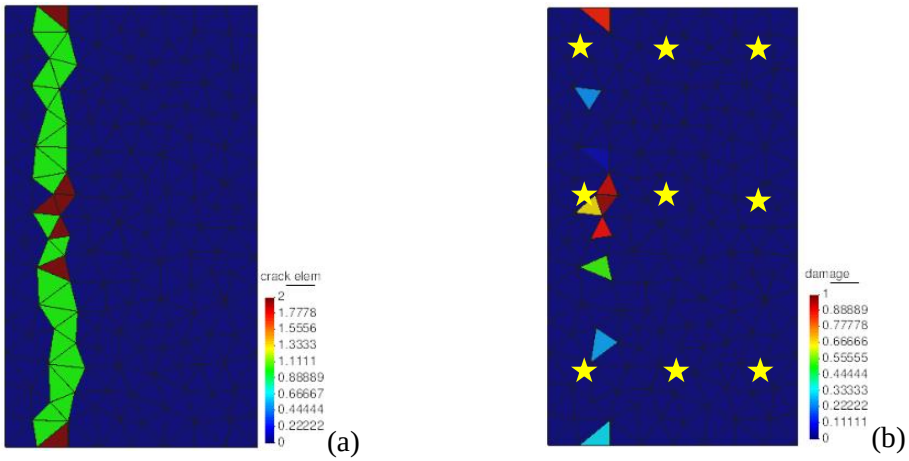

(a) (b)

Figure 7. (a) Incorporated elements and (b) elements analysed.

4.2 Uniaxial Scenario 2

For this scenario, a plan of weakness similar to the previous scenario was devised, but on the right side of the sample, Figure 8.

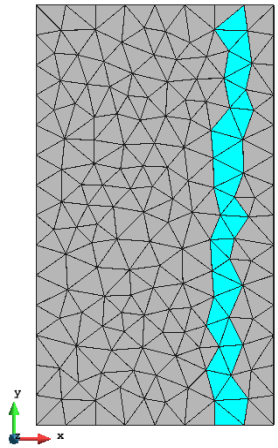

Figure 8. Position incorporated elements.

Figure 9 shows the field of displacements, 9(a) horizontal displacements and 9(b) vertical displacements, it is clear that the displacement field is larger in the region of the incorporated discontinuity. Figure 10 illustrates the stress field, 10(a) horizontal stresses, 10(b) vertical stresses and 10(c) shear stresses.

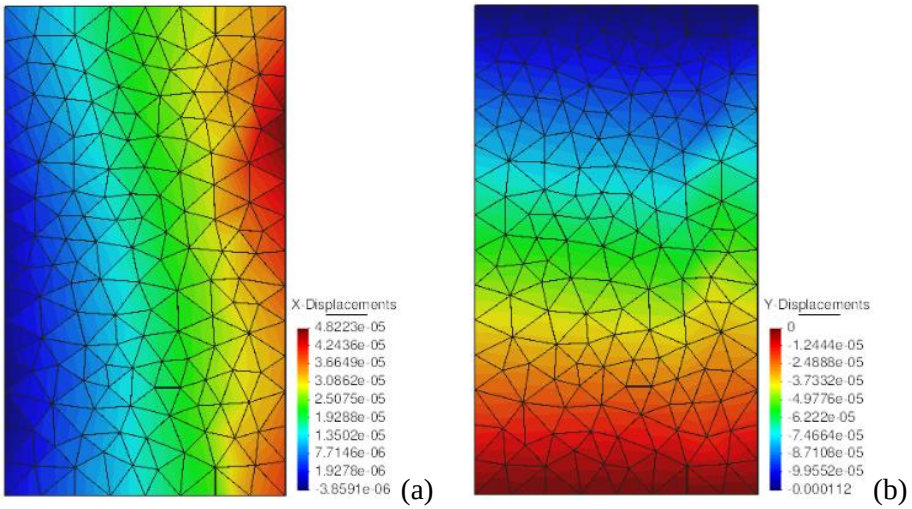

Figure 9. Field of displacement (a) Horizontal and (b) Vertical.

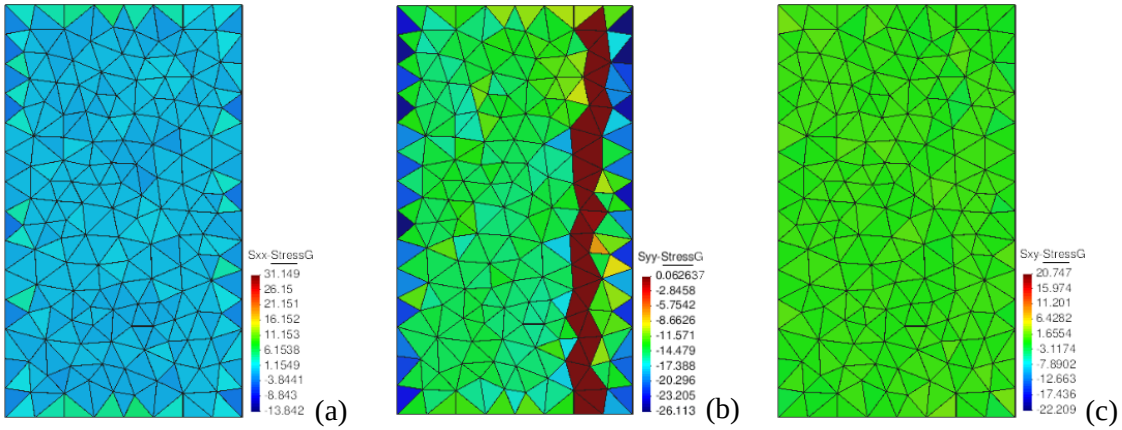

Figure 10. Stress range (a) Horizontal, (b) Vertical and (c) Shearers.

Figure 11 analyses the effect of damage on the simulation, shows that even though in a small amount there were tensile zones (Figure 11(a)) and consequently the material reaches a total material rupture (*damage = 1*) also highlights a region of degradation close to discontinuity which leads to fracture opening (Figure 11(b) and (c)).

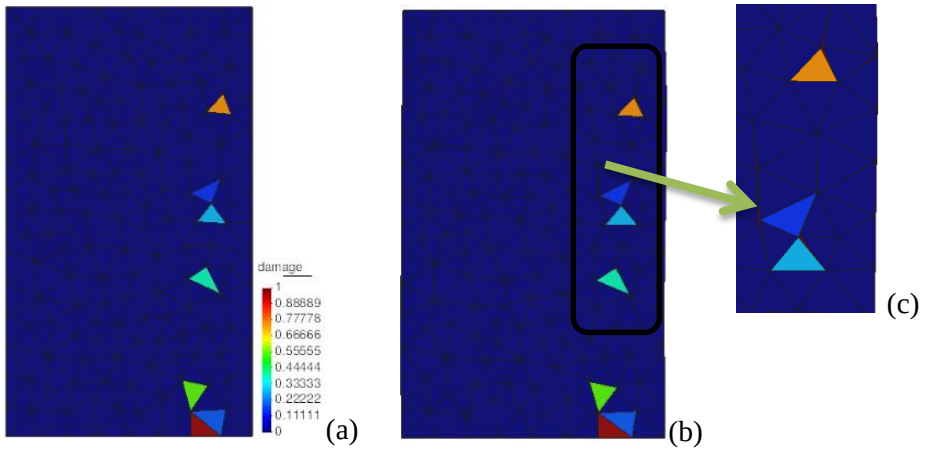

Figure 11. Damage (a) damaged elements, (b) deformed mesh at 30x scale and (c) opening detail.

And Figure 12(a) shows that the incorporated discontinuity is reactivated in localized regions, which means that there was the dilatance effect of the material. fracture opening, see Figure 12(b) called (*hjump n*).

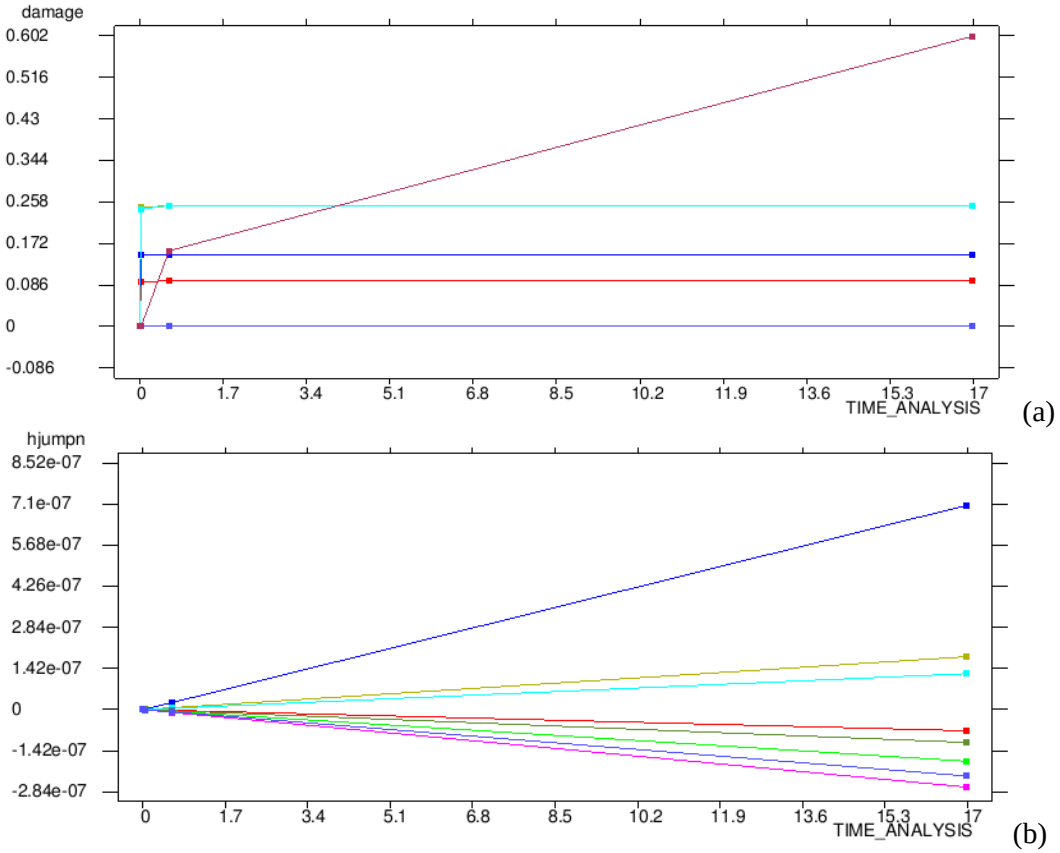

Figure 12. Evolution of (a) Damage and (b) evolution of aperture variable (*hjump n*) over time.

Figure 13(a) highlights the reactivated elements and Figure 13(b) highlights the elements that were used to generate Figures 12(a) and (b) respectively.

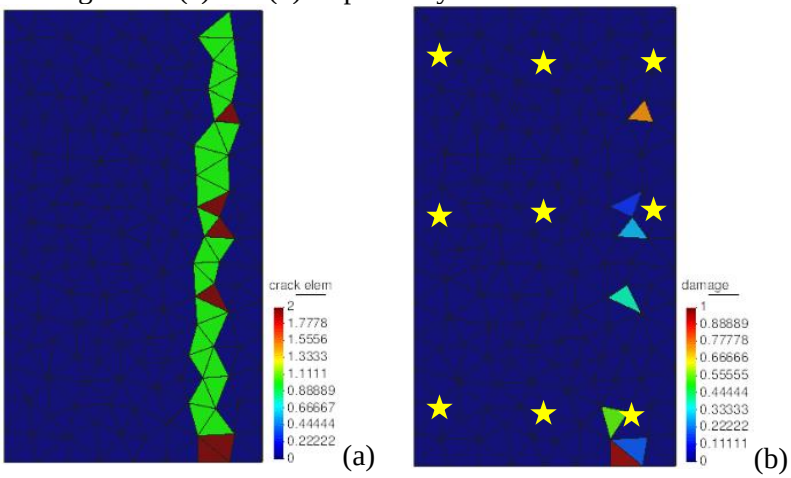

Figure 13. (a) Incorporated elements and (b) elements analysed.

4.3 Uniaxial Scenario 3

This scenario was designed with discontinuities on both sides of the sample, following to the middle of the sample, as shown in Figure 14.

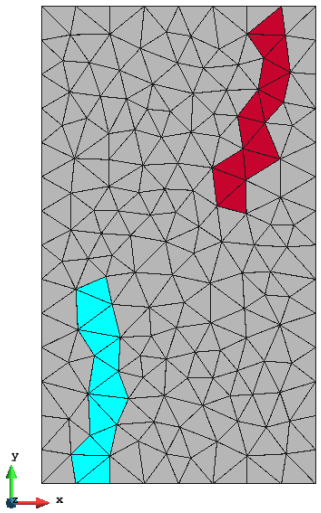

Figure 14. Position incorporated elements.

It is noted that the displacement field is characteristic of the shear effect, since the discontinuities in this analysis are located in the lower and upper region of the sample, facilitating rigid body movement. Figure 15(a) shows the horizontal offset and Figure 15(b) shows the vertical offset. Figure 16 is subdivided into three, detailing the stress field 16(a) horizontal stresses, 16(b) vertical stresses and 16(c) shear stresses.

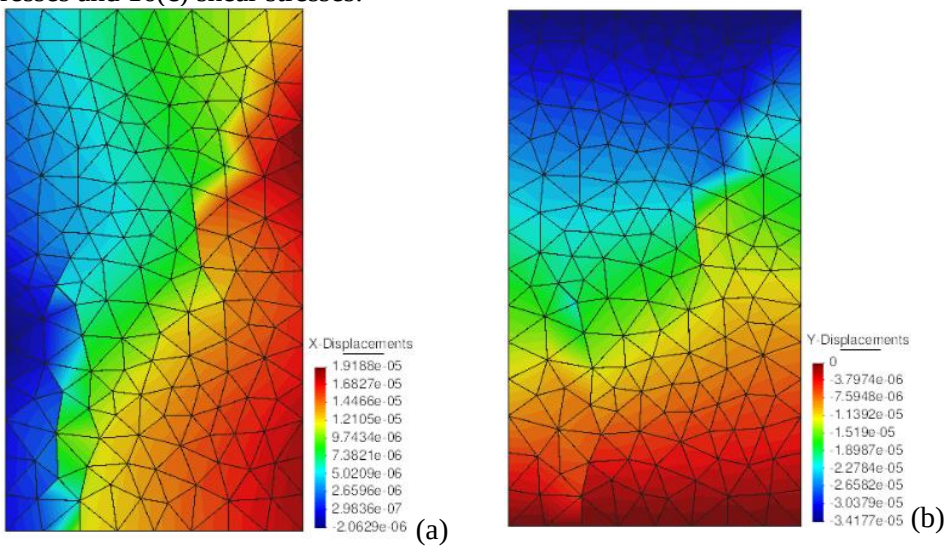

Figure 15. Field of displacement (a) Horizontal and (b) Vertical.

It is observed that the displacements, both horizontal, Figure 15(a), and vertical, Figure 15(b), present a concentration in the region of location of the discontinuities. This stress concentration is confirmed by the vertical stress concentration in Figure 16(b).

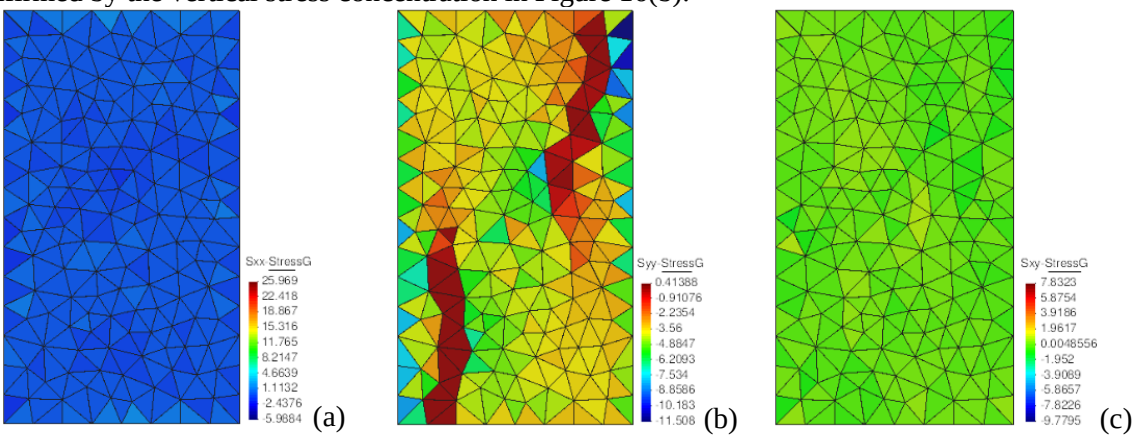

Figure 16. Stress range (a) Horizontal, (b) Vertical and (c) Shearers.

Figure 17 shows the effect of damage on the simulation, with detail for tensile zones and consequent total material rupture (*damage= 1*). In this Figure 17(b) there is also a region of degradation near the discontinuities, which leads to fracture opening.

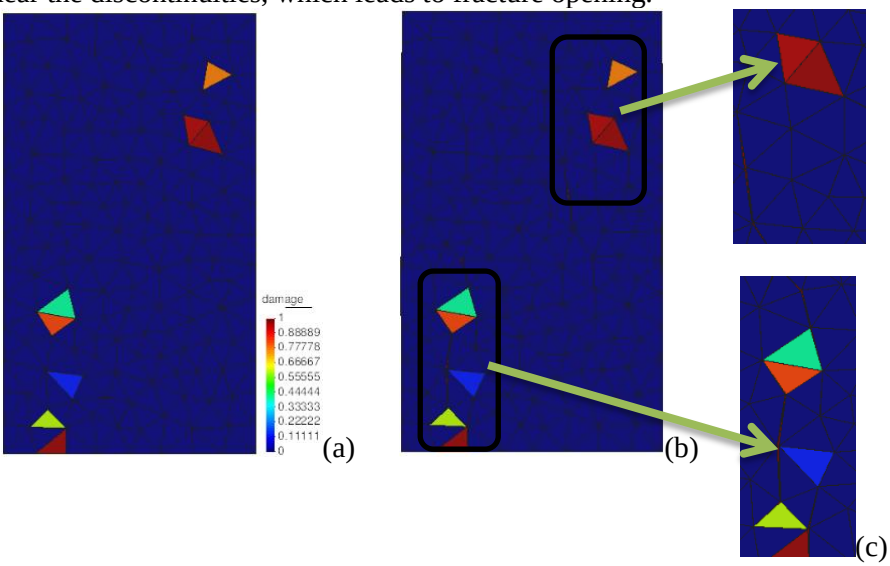

Figure 17. Damage (a) damaged elements, (b) deformed mesh at 30x scale and (c) opening detail.

The evolution of the Damage variable during simulation can be seen in Figure 18(a), while Figure 18(b) shows the evolution of the fracture opening variable (*hjump n*) over the simulation time. Figure 19 shows the incorporated discontinuity that reactivates in localized regions, similarly to the other scenarios due to the evolution of the "crack elem" variable equal to 2, which means that the material dilatance effect was observed. It is noteworthy that in the region where the elements were reactivated is precisely where the effect of fracture dilatation and opening arises, suggesting that these positions are regions of possible fracture appearance.

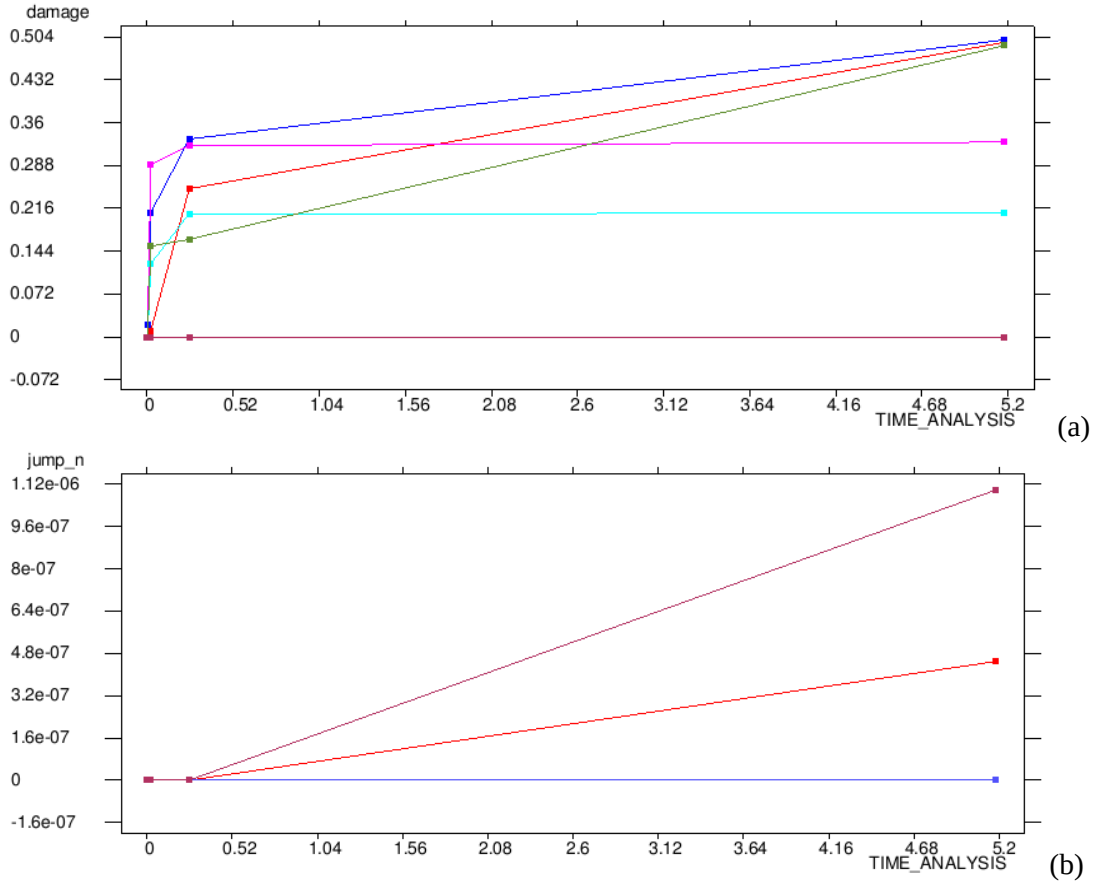

Figure 18. Evolution of (a) Damage and (b) evolution of aperture variable (*hjump n*) over time.

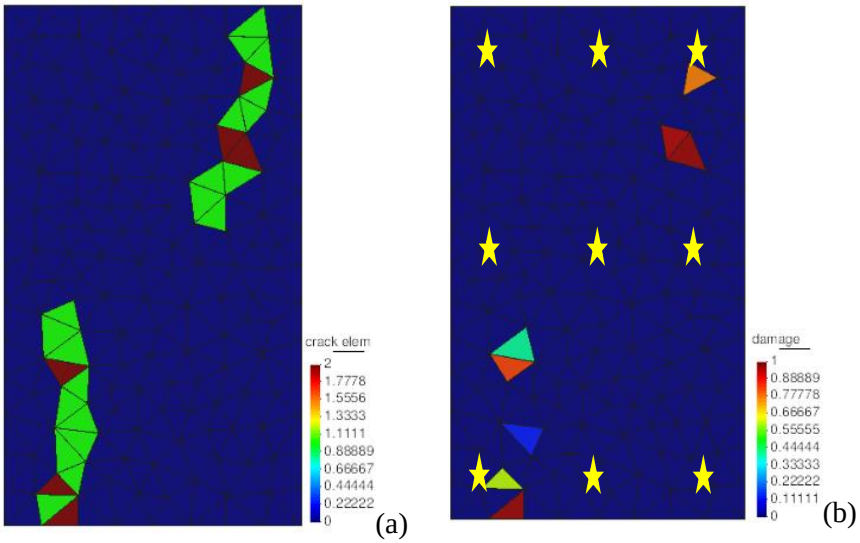

Figure 19. (a) Incorporated elements and (b) elements analysed.

4.4 Uniaxial Scenario 4

This last scenario was conceived of the discontinuity incorporated as a conjugate pair, Figure 20 presents the configuration of this scenario.

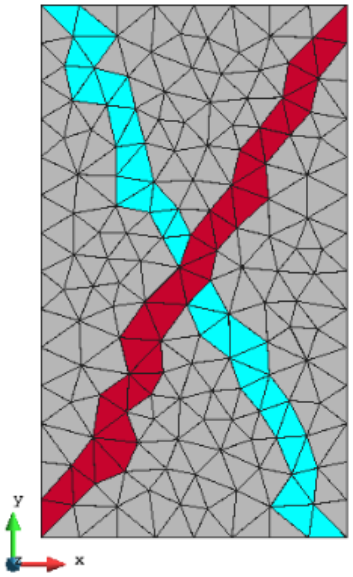

Figure 20. Position incorporated elements.

Figure 21 shows the horizontal, Figure 21(a), and vertical, Figure 21(b) offsets, where a concentration in the direction of the discontinuities can be observed. The Figure 22 shows the field of horizontal 22(a), vertical 22(b) and shear stresses, Figure 22(c).

In this Figure it can be observed the behaviour of stress distribution homogeneously in the sample, which indicates congruence with the deformations that were of the order of tenth of millimetres.

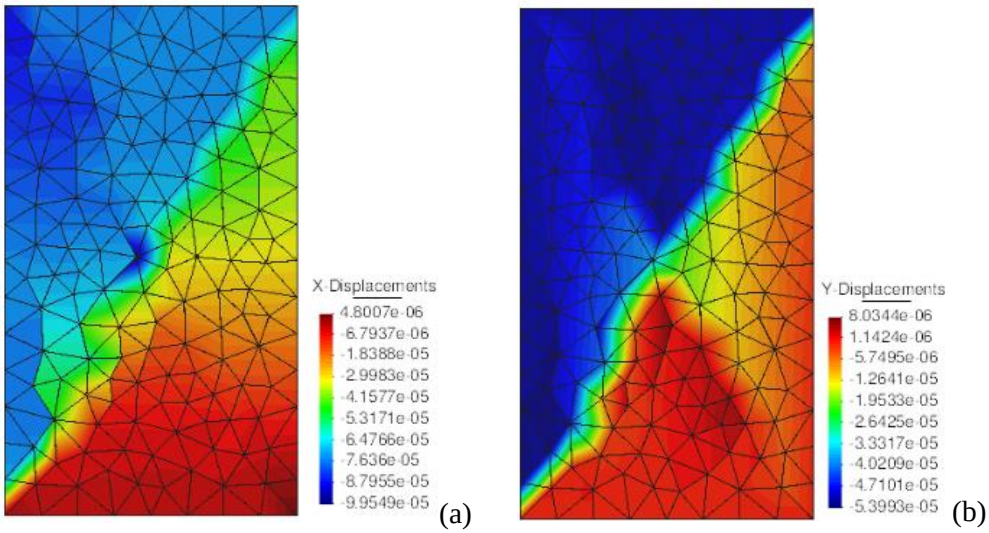

Figure 21. Field of displacement (a) Horizontal and (b) Vertical.

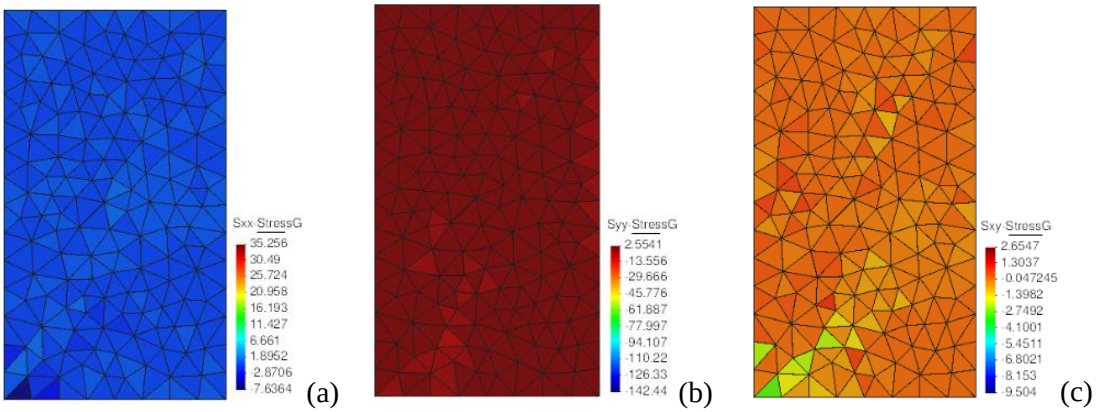

Figure 22. Stress range (a) Horizontal, (b) Vertical and (c) Shearers.

Figure 23 illustrates the effect of damage on the simulation and shows that there were tensile zones, represented by the evolution of material degradation reaching 100% in the element (*damage = 1*).

It can be observed in this image that there are embedded elements that evolve in the degradation, and, in addition, the high aspect ratio elements also present the material degradation, with the presence of openings representing the generation of fractures/cracks.

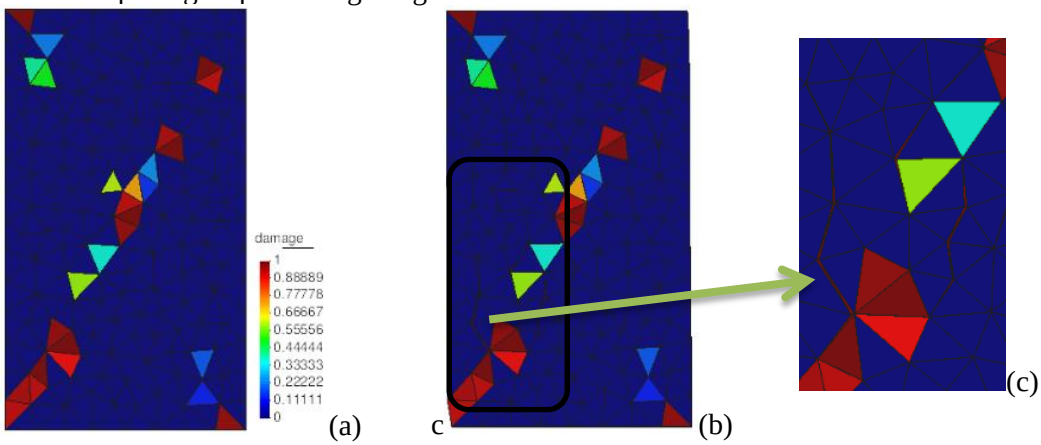

Figure 23. Damage (a) damaged elements, (b) deformed mesh at 30x scale and (c) opening detail.

Figure 24(a) shows the evolution of damage over time. In this graph it can be observed that some elements reach the maximum degradation of the material while others are still evolving.

The Figure 24(b) shows the material degradation of the incorporated discontinuity, represented by the "crack elem" variable reaching a value of 2, which means that there was a dilatant effect of the material. It is also noticed a region of degradation near the discontinuity, Figure 25(b) which causes fracture opening. Figure 25(a) shows the evolution of the fracture opening variable (*hjump n*) over time.

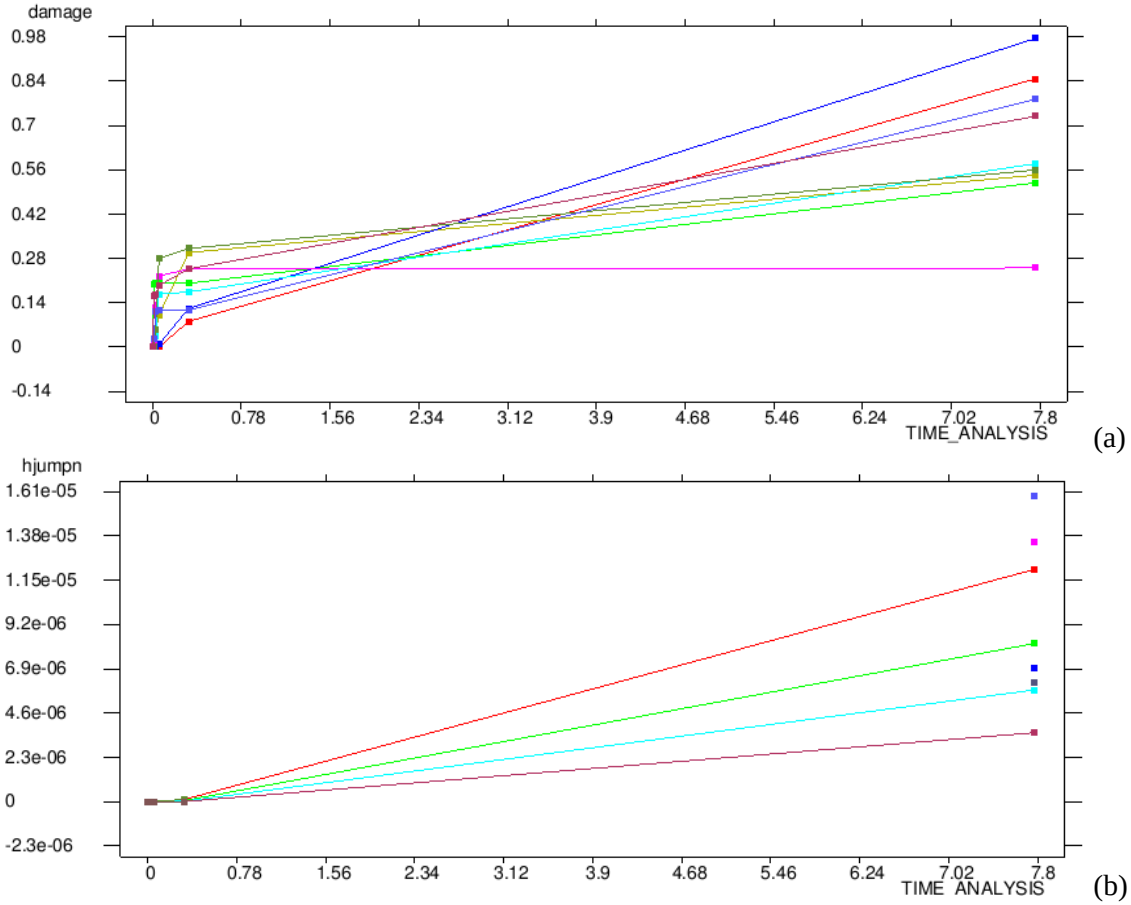

Figure 24. Evolution of (a) Damage and (b) evolution of aperture variable (*hjump n*) over time.

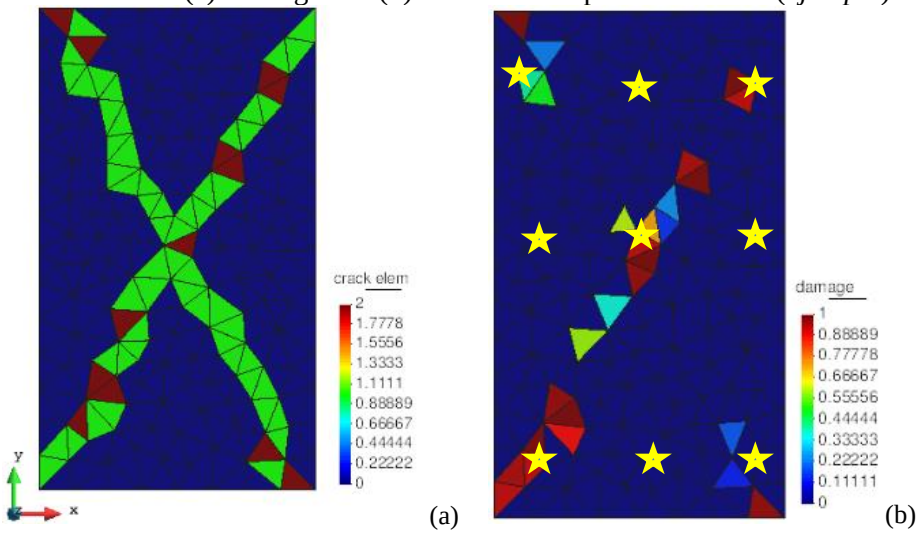

Figure 25. (a) Incorporated elements and (b) elements analysed.

5 Discussions

Observing the behavior of the evaluated scenarios, it can be noted that in all analyzes there was concentration of tensile stresses and consequent degradation of the material.
Comparing the behavior of the evaluated scenarios, it can be observed that the second and third scenarios reached higher shear stresses than the others, this being a scenario that represented a rock sample with a vertical weakness plane.

In scenarios 3 and 4, the weakness plans allowed the sample to have the expected shear behavior, with weakness plans that crossed the sample diagonally in both analyzes. Especially in scenario 4, weakness plans ended up connecting across the field of displacements, with voltages reaching lower values than all other scenarios.

These analyzes suggest that pre-existing planes of weakness in rock samples are susceptible to stress concentration and premature tensile fracture opening, possibly reducing the strength of materials in uniaxial compression.

6 Conclusions

Given the analyses performed, it can be seen that besides the expected behaviour of the material during the uniaxial test, tensile stress zones can be observed throughout the sample.

Therefore, this paper shows the tendency, in a state of uniaxial compression, of rocks with weakness planes to tend to generate tensile stress zones, which may cause crack formation or dilatation effect.

Thus, this work concluded that for research purposes and efficiency in the sizing of engineering works, this methodology highlights the importance of tensile stress investigation and its influence on compressive environments.

Acknowledgements

To the GeomeCCarb research project: Study of Geomechanical and Geochemical Couplings in Carbonate Reservoirs, for financial support. The Laboratory of Computational Methods in Geomechanics for the support for the development of this work.

References

BŁAŻEJCZAK, D.; ŚNIEG, K.; SŁOWIK, M. Comparison of Proctor and Uniaxial Compression Tests for Selected Soils. **Agricultural Engineering**, v. 22, n. 1, p. 5–13, 2018.

FAKHIMI, A.; HEMAMI, B. Rock Uniaxial Compression Test and Axial Splitting. **Procedia Engineering**, v. 191, p. 623–630, 2017.

HOLZHAUSEN, G.R. & Johnson, A.M. (1979) Analyses of longitudinal splitting of uniaxially compressed rock cylinders, Int. J. Rock Mech. Min. Sci. Geomech. Abstr. 16, 163–177.

KAKLIS, K. N. et al. Experimental investigation of the mechanical properties of Alfas stone. **Frattura ed Integrita Strutturale**, v. 11, n. 40, p. 18–32, 2017.

MATHEUS MONTES PIMENTA; ANDRE CEZAR ZINGANO; FERNANDO ALVES CANTINI CARDOZO. Comportamento De Rochas Sob Carregamento Cíclico Em Ensaios De Compressão. **Anais do VII Simpósio Brasileiro de Mecânica das Rochas**, n. November, 2016.

OLIVER, J. et al. **Two-dimensional modeling of material failure in reinforced concrete by means of a continuum strong discontinuity approach**. Comput. Methods Appl. Mech. Engrg, 197 (2008) 332-348.

SÁNCHEZ, M., MANZOLI, O. L.; GUIMARÃES, L. **Modeling 3-D desiccation soil crack networks using a mesh fragmentation technique**. Computers and Geotechnics, 62, 27–39.2014.

SIMO; JU. **Stress and strain based continuum damage models: I Formulation.** Int. J. Solids Struct, 15 (1987) 821–840.

RODRIGUES MARQUES, Í. et al. Análise comparativa de resultados de ensaios de compressão triaxial com corpos de prova de diferentes dimensões. **Revista Tecnologia**, v. 35, n. 1/2, p. 66–77, 2017.